bezell house, inc.
JOURNAL PRODUCTION DEPARTMENT

22292 Calibre Court, #1607
Boca Raton, FL 33433
561-750-0941 (Voice)
561-504-0556 (Messages)
508-590-5860 (e-Fax)
anaturewalk@earthlink.net

H. L. Clack
Department of Mechanical, Materials, and Aerospace Engineering
Illinois Institute of Technology
10 West 32nd St.
Chicago, IL 60616-3793

Article Reference: AAS-444

Date Proof Sent: 4/13/04

Correction Deadline: **4/19/04**

Total Pages: 23

Journal: ATOMIZATION & SPRAYS

Year: 2004 **Vol. 14** **Issue 3**

Article Title: "DEVELOPMENT OF AN AIR-BLAST ATOMIZER FOR INDEPENDENT CONTROL OF DROPLET SIZE AND SPRAY DENSITY"

Dear Professor Clack:

Attached is a PDF file containing the author proof of your article. If you are unable to access this file, please let me know and I will fax your proof. Please return your corrections in one of the following ways: (1) *Fax*: Clearly mark your corrections on the page proofs and fax the **corrected pages only**, along with the offprint order form, if applicable. (2) *E-mail:* Indicate your corrections in a list, specifying the location of the respective revisions as precisely as possible. Please **DO NOT** annotate the PDF file. Thanks.

Please read the edited paper carefully, making certain that your meaning and the accuracy of the data are unchanged. Answer copyeditor's queries in the margin. Failure to answer queries will result in the delay of publication of your article, so please make sure they are all adequately addressed.

Please send, by the "Correction Deadline" above, either your corrections or your notification that you have reviewed the proof and have no corrections. If we do not hear back from you by the deadline, we will be happy to hold your article for a future issue, to give you more time.

Please note that this is your only opportunity to review the editing, typesetting, figure placement, and accuracy of text, tables, and figures. There is no charge for corrections to editorial or typesetting errors. You *will* be billed at the rate of $25 per hour of production time, however, for rewriting, rewording, or otherwise revising the article from the version accepted for publication ("author alterations"). Any such charges will be invoiced and must be paid *before* the article is published.

Attached is a form for ordering offprints, issues, or a subscription, as well as a 2004 B&W Offprint Pricing chart, including a formula to calculate the price of extra "color" offprints. As corresponding author, you will receive a complimentary copy of this issue. If you wish to order extra issues or offprints, please fill in the appropriate areas and fax the form to me with your corrections.

Thank you for your assistance, and please reference **AAS-444** in your correspondence. Also, kindly confirm receipt of your proofs. No article will be published without confirmation of the author's review.

Thank you,

Marje

Marje Pollack
Production Editor

begell house, inc.
JOURNAL PRODUCTION DEPARTMENT

22292 Calibre Court, #1607
Boca Raton, FL 33433
561-750-0941 (Voice)
561-504-0556 (Messages)
508-590-5860 (e-Fax)
anaturewalk@earthlink.net

ARTICLE REFERENCE #AAS-444
(use in all correspondence)

YEAR: 2004 VOLUME 14 ISSUE 3

Dear Professor Clack:

As corresponding author, you will receive a complementary copy of this issue. If you wish to order extra offprints of your article, copies of the issue, or subscriptions to the volume, please circle the appropriate box(es) below. You may also indicate your willingness to pay for color printing of figures, if applicable.

Please return this form with your corrected proof. **If sending payment with the order, please include cost of shipment as indicated below, make check payable to Begell House, Inc.,** and mail to the above address. If a purchase order is required, it may arrive separately to avoid delaying the return of the corrected proofs.

OFFPRINTS OF ARTICLE*

PAGE COUNT: 24 (BLACK AND WHITE)

QUANTITY:		QUANTITY:	
	050		1000
	100		1500
	200		2000
	300		3500
	400		5000
	500		7500
	750		10,000

See attached for additional color offprint charge.

AUTHOR DISCOUNTS ON COPIES OF ISSUES

RANGE	AUTHOR PRICE PER ISSUE	QTY
01	$ 12.92	

COLOR PRINTING (IF APPLICABLE)

Check appropriate box according to number of color pages desired (refer to author proof for calculating pages)

1 page: $ 1,200 ☐

SUBSCRIPTION — 2004

INSTITUTIONAL $ 432.00
INDIVIDUAL $ 85.50

For shipment outside the Continental US, add $10/issue.

*Add 20% for shipment of offprints.

WIRE TRANSFER

Bank: **Valley National Bank**
Routing #: **0 2600 6 790**
Account #: **07 011343**

CREDIT CARD PAYMENT

CREDIT CARD #

NAME ON CREDIT CARD

AMEX/ VISA/MC/ DISC/ EURO/ EXP.

OTHER: _____

Fax or mail this form to Begell House, Inc.

CHECK PAYMENT

INCLUDE THE FOLLOWING INFORMATION ON THE CHECK:

AAS/1403/444

Make check payable to Begell House, Inc.

CORPORATE PURCHASE ORDER

P. O. #

Fax or mail this form to Begell House, Inc.

2004 BLACK & WHITE OFFPRINT PRICING (includes cover)

Shipping - add 20% to black & white charge

Color - add $3.00 per color page X offprint quantity being ordered

Page count of article (round off to highest multiple of 8)

Quantity	4	8	16	24	32	40	48	56	64	72	80	88	96	104
25	63	100	131	163	194	221	252	284	315	352	368	394	415	431
50	73	110	142	173	205	236	268	299	331	362	383	404	425	446
100	94	168	221	273	326	378	431	483	536	588	630	672	714	756
200	136	284	378	473	567	662	756	851	945	1,040	1,124	1,208	1,292	1,376
300	178	399	536	672	809	945	1,082	1,218	1,355	1,491	1,617	1,743	1,869	1,995
40	220	515	693	872	1,050	1,229	1,407	1,586	1,764	1,943	2,111	2,279	2,447	2,615
500	262	630	851	1,071	1,292	1,512	1,733	1,953	2,174	2,394	2,604	2,814	3,024	3,234
750	367	919	1,244	1,570	1,895	2,221	2,546	2,872	3,197	3,523	3,838	4,153	4,468	4,783
1,000	473	1,208	1,638	2,069	2,499	2,930	3,360	3,791	4,221	4,652	5,072	5,492	5,912	6,332
1,500	683	1,785	2,426	3,066	3,707	4,347	4,988	5,628	6,269	6,909	7,539	8,169	8,799	9,429
2,000	893	2,363	3,213	4,064	4,914	5,765	6,615	7,466	8,316	9,167	10,007	10,847	11,687	12,527
3,500	1,523	4,095	5,576	7,056	8,537	10,017	11,498	12,978	14,459	15,939	17,409	18,879	20,349	21,819
5,000	2,153	5,828	7,938	10,049	12,159	14,270	16,380	18,491	20,601	22,712	24,812	26,912	29,012	31,112
7,500	3,203	8,715	11,876	15,036	18,197	21,357	24,518	27,678	30,839	33,999	37,149	40,299	43,449	46,599
10,000	4,253	11,603	15,813	20,024	24,234	28,445	32,655	36,866	41,076	45,287	49,487	53,687	57,887	62,087

Atomization and Sprays, vol. 14, pp. xx–yy, 2004

[[AU: FIGURES HAVE BEEN RENUMBERED. PLS. CONFIRM ACCURACY. ALSO, PLS. CHECK "CHARACTERS" CAREFULLY, TOO. THANK YOU.]]

DEVELOPMENT OF AN AIR-BLAST ATOMIZER FOR INDEPENDENT CONTROL OF DROPLET SIZE AND SPRAY DENSITY

*H. L. Clack**
Department of Mechanical Engineering, University of California, Berkeley, Berkeley, California, USA

C. P. Koshland
School of Public Health, University of California, Berkeley, Berkeley, California, USA

D. Lucas
Lawrence Berkeley National Laboratory, University of California, Berkeley, Berkeley, California, USA

R. F. Sawyer
Department of Mechanical Engineering, University of California, Berkeley, Berkeley, California, USA

The atomizer described is a novel twin-fluid design that allows independent control of mean droplet size and mean spray density. Designed to handle unpressurized fluids at low flow rates, the prefilming double-annular air-blast atomizer (PFDAAA) distributes fuel in a liquid film over a hollow, tapered cylindrical centerbody. Two independently controlled atomizing gas streams shear the inner and outer surfaces of the cylindrical fluid film at the injector tip, resulting in continuously variable atomization. Data taken during a series of cold-flow experiments include both mean droplet size and spray density measures. The data demonstrate that controlling the relative flow rates of the two atomizing gas streams produces droplet dispersions whose mean droplet size and spray density vary independently of each other. Measured values of Sauter mean diameter (SMD) for isopropyl alcohol sprays range from 250 to 3100 μm, and values of normalized interdroplet spacing range from 0.8 to 3.6 mean droplet diameters. When presented collectively, the mean droplet size and spray density data form a performance map indicating the operating range of the PFDAAA for the conditions tested. Parametrically variable sprays such as those generated by the PFDAAA constitute a previously unavailable experimental platform for spray combustion research. Investigations using laser diagnostics to probe a controlled, variable spray could provide insights into the physicochemical processes within a spray that ultimately affect combustion efficiency and pollutant formation.

INTRODUCTION

Before the development of laser-based anemometry, velocimetry, holographic imaging, and "rainbow" thermometry spray diagnostic techniques, investigators were limited in their

This research was supported by the Environmental Health Sciences Superfund Basic Research Program (Grant P42 ESO 47050-01). The authors thank Prof. Carlos Fernandez-Pello and the creators of ImageTool for their material contributions to this work.

*Corresponding author; current address: Department of Mechanical, Materials, and Aerospace Engineering, Illinois Institute of Technology, 10 West 32nd St., Chicago, Illiniois 60616-3793, USA.

means of studying spray combustion phenomena. The very nature of sprays and spray combustion makes spray properties extremely difficult to measure. Partially in response to this reality, investigators have often chosen instead to isolate and study specific phenomena at the droplet scale. Studies have examined a variety of droplet phenomena, providing validating data for numerical models and revealing the basic mechanisms underlying dilute spray behavior. Rayleigh [1] and Taylor [2, 3] used a stability analysis approach to address droplet formation, laying the basis for many subsequent investigations [4–10] on drop formation in sprays. Studies have also focused on the different transformations that droplets undergo within the spray, including droplet deformation and secondary breakup [11–13], and droplet bounce, collision, coalescence, and separation [14–16]. Godsave [17] and Spalding [18] studied the basic vaporization behavior of a single droplet, leading to the d^2 law. Subsequent droplet vaporization and burning experiments have incorporated the effects of multicomponent fuels [19–21] and used droplet streams and arrays [22, 23] and counterflow spray diffusion flames [24, 25] to explore the burning behaviors of droplet clusters. Droplet combustion modeling has included analytical descriptions of group combustion behavior [26–28] as well as numerical simulations of burning droplet streams, arrays, and clusters [29–32]. Detailed heat and mass transfer calculations for droplets within various droplet cluster configurations have been reported [33, 34], as well as the effects of multicomponent fuels on droplet vaporization, ignition, and combustion [35–39]. The insights gained from droplet-scale investigations, however, can be difficult to extend to practice. Such studies often examine phenomena *ex situ*, imposing spatial symmetry, well-defined boundary conditions, and other idealized characteristics to facilitate computational modeling or the collection and interpretation of experimental data. Such conditions, however, are rarely representative of realistic sprays, thus limiting the applicability of the results.

Variable sprays produced by controlled atomization represent an experimental platform for addressing some of these issues. Variable sprays provide an opportunity to study how changes in one spray characteristic affect other spray characteristics and the behavior of the overall droplet dispersion. These goals differ substantially from those of previous atomization studies, which largely characterized nominal [40–43] or off-design [44–46] atomizer performance, or explored new atomization concepts [47–49] or performance-enhancing design modifications [50–52]. The advantages of variable sprays become clearer in the context of studying spray combustion phenomena. Large temperature and species gradients that exist within a burning spray can strongly influence droplet vaporization, combustion chemistry, and pollutant formation. Interacting droplets within dense sprays can induce local maxima and minima in the gas-phase temperature and species distributions that further compound this effect. By inducing variations in the bulk properties of sprays, further insight may be gained into the group behavior of droplet dispersions and the internal physicochemical structure of vaporizing and combusting sprays. Previous studies [53–55] used the current atomizer for precisely this purpose: to evaluate how spray properties influence the formation of toxic products of incomplete combustion (PICs) during liquid hazardous waste incineration. The data from these studies indicate that variations in the mean droplet size or droplet number density of a vaporizing, solid-cone spray could produce different results [53, 54] than those obtained in earlier studies of vaporizing linear droplet streams [56, 57]. The two different results lend support to the assertion that variable sprays may reveal evidence of droplet phenomena that more fundamental droplet experiments do not. If controlled atomization were used in conjunction

with current spray diagnostics and numerical modeling capabilities, the three could form a particularly effective investigative approach: physically realistic, parametrically variable, solid-cone sprays; probed with laser-based diagnostics to obtain spatially resolved property data within the spray; and modeled using the latest numerical algorithms for droplet cluster vaporization, ignition, and burning.

EXPERIMENTAL DESIGN

This novel injector design resulted from efforts to study the effects of atomization quality on liquid hazardous waste incineration [53–55]. The injector was designed to operate within a vertically oriented combustion-driven flow reactor, shown schematically in Fig. 1. The injector operates in the postflame region of the flow reactor, thereby producing sprays that vaporize but do not necessarily ignite. This configuration facilitates the study of by-product formation resulting from combustion instabilities during liquid hazardous waste incineration. Such instabilities can cause incomplete vaporization of the atomized liquid waste within the flame zone, resulting in vaporization and thermal decomposition of the waste in the postflame region. The injector design reflects the many physical constraints associated with its operation in the flow reactor: a small cross section relative to the 8.26-cm flow reactor diameter; minimal disturbance of the reactor temperature and velocity profiles; injection of liquids in the hot reactor environment without promoting premature vaporiza-

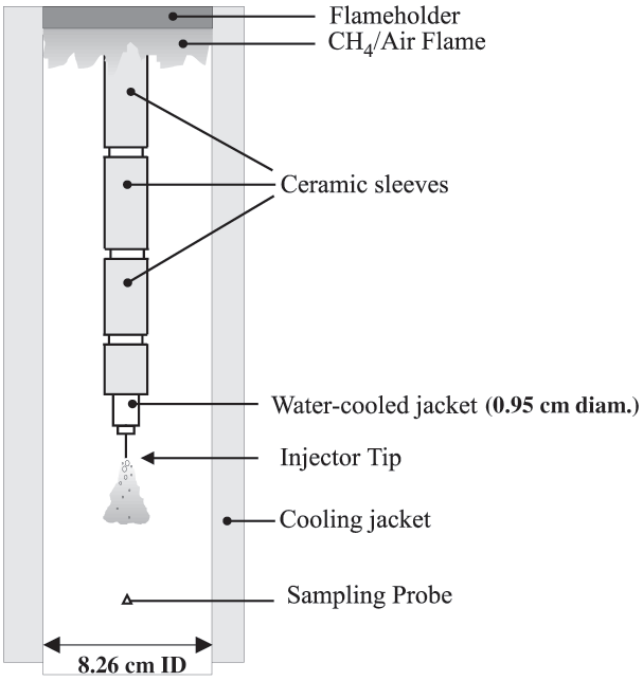

Fig. 1 Installation of PFDAAA in vertical combustiondriven flow reactor, suitable for studies of postflame spray vaporization and chemistry (drawing not to scale).

tion; and material durability in the high-temperature, corrosive reactor environment. Within these constraints, the target performance of the atomizer was droplet dispersions having Sauter mean diameters (SMD) of 300 μm or less at a flow rate of approximately 1 ml/min. Pressure-driven atomization is not realistic because of the small orifice diameter required by the low liquid flow rate and small droplet size. The harsh environment and small cross section preclude the use of piezoelectric droplet generators. Consequently, the design and performance data presented here represent a solution that achieves the desired injector performance, given the constraints of the operating environment and the existing apparatus.

The resulting design is a prefilming double-annular air-blast atomizer (PFDAAA) capable of independent variation of spray mean droplet diameter and spray mean droplet density. Shown schematically in Fig. 2, it consists of a hollow-needle centerbody (1.59 mm OD), centered within a 3.18-mm-OD stainless steel tube, both of which are centered within a 6.35-mm-OD stainless steel tube. Separately metered streams of nitrogen gas flow through the hollow-needle centerbody and the outer annulus. The liquid injectant flows through the inner annulus, forming a film over the hollow-needle centerbody. Nitrogen gas flowing through the outer annulus ("annular gas flow") drives the liquid film toward the tip of the needle centerbody, where ligaments form, and provides a sheath flow of gas to inhibit droplet dispersion. The flow of nitrogen gas through the tip of the hollow-needle centerbody ("needle gas flow") completes the atomization process, and enhances droplet dispersion. By independently varying the volumetric flow rates of the two nitrogen

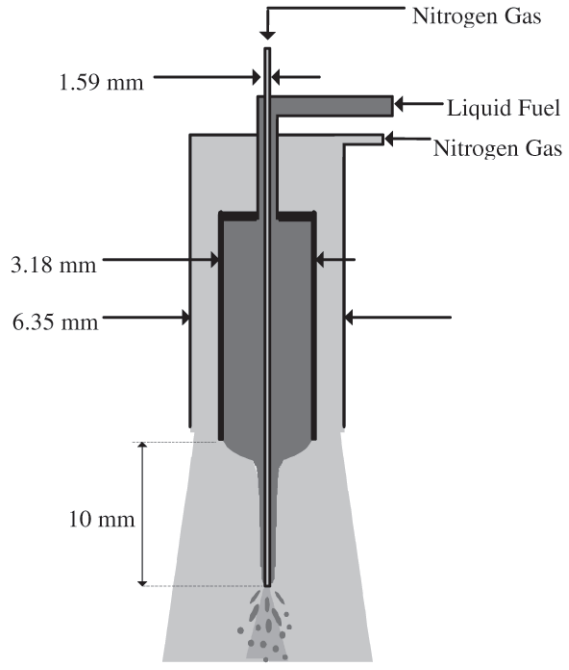

Fig. 2 Schematic of the prefilming double-annular air-blast atomizer (PFDAAA) (drawing not to scale).

gas streams, atomization continuously varies from a mostly air-blast process (annular gas flow dominates) to a mostly air-assist process (needle gas flow dominates). Active water cooling prevents premature vaporization of the injectant while it is flowing through the injector. Fiberfrax-lined ceramic sleeves encase the injector to prevent the development of thermal boundary layers that would lower downstream temperatures in the flow reactor.

Injectants tested included water, isopropyl alcohol, and 1,1,1-trichloroethane (TCA). That TCA is one of the injectants reflects its central role as a hazardous waste surrogate in the combustion studies [53–55] that prompted PFDAAA development. The most extensive data exist for isopropyl alcohol, because its fluid properties are most similar to those of TCA (see Table 1), while posing less of a health risk. Water is problematic, mainly because its high surface tension causes droplets to form at the exit plane of the 3.18-mm-OD tube, rather than forming a continuous film along the centerbody. Selected dyes added to the injectants increase spray opacity and improve droplet imaging. Fluorescein dye provides adequate opacity for water and isopropyl alcohol sprays (concentrations of 0.5 g/500 ml), while Pyrromethene 597 dye (Exciton Corp, Dayton, OH) dissolves in and performs well for TCA sprays. All liquids are filtered and supplied to the injector by a high-precision Rabbit HP solvent delivery pump at a volumetric flow rate of 1 ml/min. This low injectant flow rate assures that concentrations of gas-phase combustion by-products in the flow reactor do not exceed the detection limits of the infrared absorption instrument.

A series of cold-flow experiments was conducted in an enclosed and ventilated quartz spray chamber (Fig. 3) to characterize the performance of the PFDAAA. The chamber consists of a 13.34-cm-diameter quartz T-joint, with the PFDAAA oriented downward in the main branch and the cross branch providing undistorted optical access for the video camera. A strobe lamp operating at 60 Hz with a flash duration of approximately 0.6 μs illuminates the spray through the quartz at right angles to the video camera. The light from the strobe passes through a slotted lens cover (4-mm opening), producing a light sheet. The light sheet passes through a cylindrical lens (76.2-cm focal length) on the near side of the spray chamber that focuses the light sheet on the injector axis. A mirror positioned on the far side of the spray chamber reflects the light sheet back through the spray, to provide more even illumination. Light shields surrounding the transparent spray chamber are covered in black felt to provide a dark background and to eliminate unwanted reflections.

A Sony Hi-8 video camcorder recorded the spray images, which were then played back on a television monitor to select and acquire specific frames using a Snappy Video Snapshot peripheral device. The camcorder zoom, a telescopic lens, and the 26-in. television monitor together provide 40:1 magnification of the spray and a maximum resolution of 14 μm, calibrated by imaging a fine-scale ruler. For the results reported here, the field of view encompasses the region immediately downstream of the injector tip and measures

Table 1 Fluid Properties of Various Injectants

	Density [kg/m^3]	Viscosity (@ K) [poise]	Surface tension (@ K) [dyn/cm]
Water	1000.0	0.01 (293)	73.05 (291)
Isopropyl alcohol	785.1	0.029 (288)	23.71 (293)
TCA	1349.2	0.012 (293)	25.8 (293)

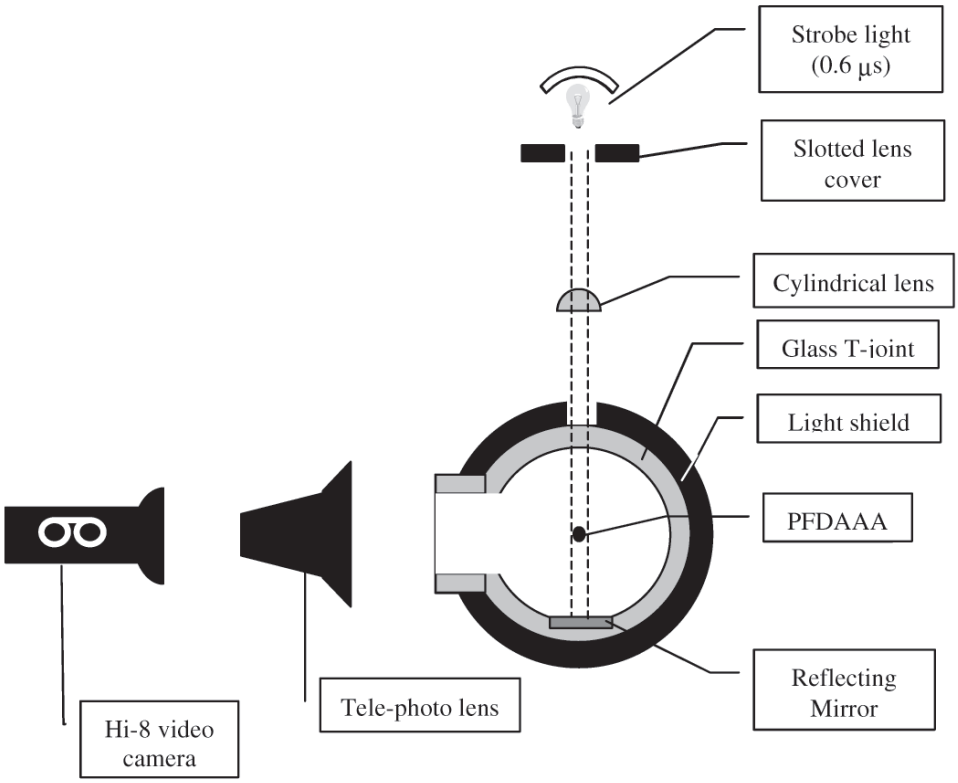

Fig. 3 Schematic of experimental apparatus (top view, not drawn to scale).

14.6 mm by 11.0 mm with a depth of field of 4–5 mm. ImageTool[1] software analyzes the acquired images and calculates the equivalent diameter and centroid coordinates for each droplet, omitting any incompletely atomized liquid "ligaments" that may be present.

Several confidence tests were conducted to validate the spray analysis method. Operator bias was evaluated in the following manner. Twenty images were analyzed twice. The first analysis was intentionally cursory. The sample included droplets that were out of focus or partially obscured by glare. Also included in the sample were coalescing or incompletely atomized droplets attached to ligaments. The second image analysis was conducted more carefully, rejecting some droplets that were accepted in the first analysis. The higher rejection rate of the second analysis produced a 62% smaller sample size, but resulted in only a 7% difference in the calculated SMD between the two samples, indicating that operator bias is not a significant source of error. Aggarwal and Shuen [59]**[[AU: ADD TO REFERENCES LIST]]** conclude that SMD is a sufficiently accurate representation of the complete droplet size distribution for vaporizing sprays.

The effect of sample size was evaluated by comparing SMD and size distributions for sample sizes of 117 and 196 counts. Although the distribution of the smaller sample

[1]ImageTool image processing and analysis software was developed at the University of Texas Health Science Center, and can be downloaded for free from http://www.uthscsa.edu.

exhibited a slight shift to larger droplet sizes, this resulted in less than a 2% difference in SMD.

Finally, calculating the ferret diameter of droplet from an image is problematic for aspherical droplets where the eccentricities do not occur in the plane of the image. We reason that volume-increasing ("bulges") and volume-decreasing ("dents") asphericities occur randomly. As a result, the net error that they induce will decrease as sample size increases.

RESULTS AND DISCUSSION

The two quantities used to parameterize PFDAAA performance and atomization quality are the spray mean droplet size and the spray density. The selection of mean droplet size reflects the influence that droplet size has on droplet transport and vaporization behavior, particularly for spray combustion applications. Mean droplet sizes reported here are in the form of Sauter mean diameter (SMD). Sauter mean diameter is a D_{32} weighted mean that represents the diameter of a droplet whose volume-to-surface area ratio equals that of the entire spray. Spray density serves as a measure of the degree to which droplets in a droplet dispersion behave independently.

Distances between neighboring droplets decrease as spray density increases, increasing the likelihood that interactions will occur between the heat, momentum, and energy transfer processes of neighboring droplets. The mean value of these distances within a spray serves as the basis for several measures of spray density, described in further detail in the Results and Discussion section and in the Appendix.

Spray Mean Droplet Size Measurements

Shown in Fig. 4 is a sample image, along with its binary counterpart, of the sprays generated by the PFDAAA. Representative count and volume fraction distributions for TCA sprays are shown in Fig. 5 for the most dense and most dilute cases.

The influences of the annular and needle gas flows on the SMD of the resulting sprays are evident for isopropyl alcohol in Fig. 6 and Fig. 7. Figure 6 shows the variation

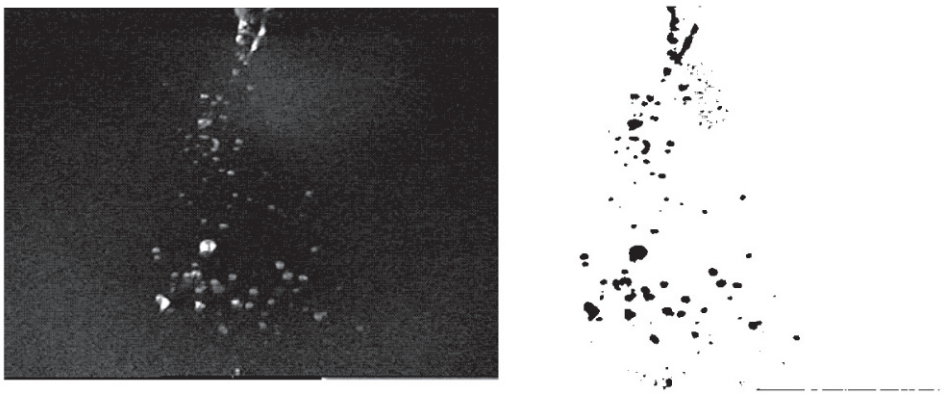

Fig. 4 Sample image before and after processing.

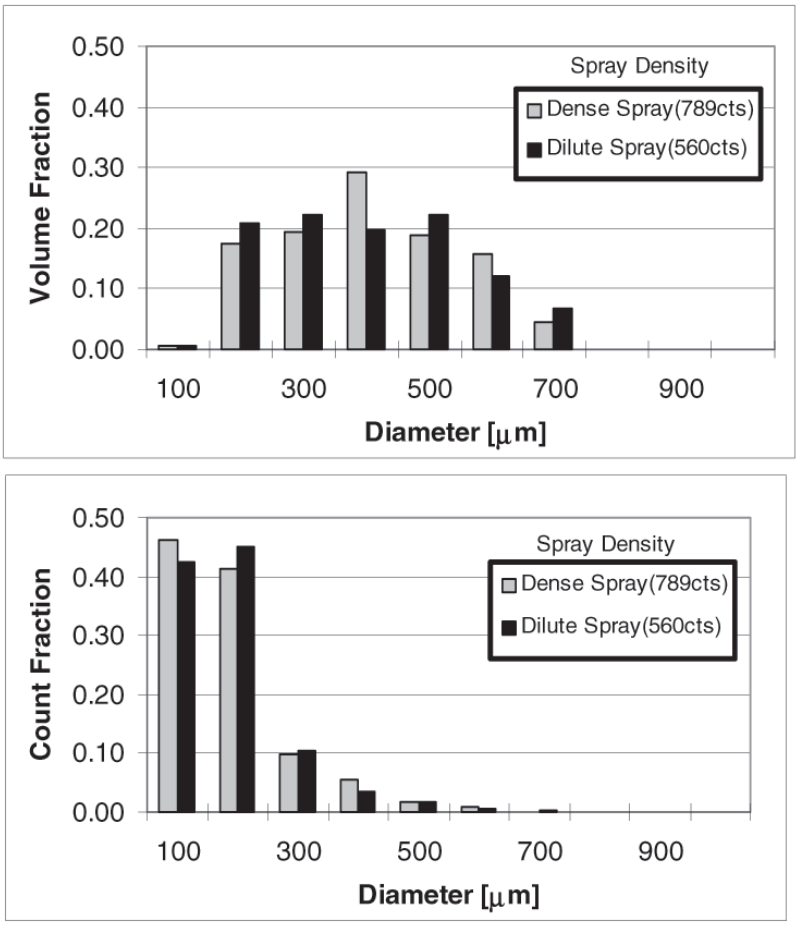

Fig. 5 Representative count and volume fraction distributions for dense and dilute PFDAAA-generated TCA sprays (mean droplet diameter for both cases is fixed at SMD ≈ 265–280 μm).

in SMD with annular gas flow rate for three different series of needle gas flow rates. The complementary results in Fig. 7 show the variation in SMD with needle gas flow rate, at five different series of annular gas flow rates. The data in Fig. 6 and Fig. 7 are combined in Fig. 8 to show the full range of Sauter mean diameter values produced by the PFDAAA for the conditions tested. The dual-mode nature of the atomization process is evident in Fig. 6 and Fig. 7. In Fig. 6, the variation in SMD for the case with no gas flow through the hollow-needle centerbody decreases monotonically with increasing annular gas flow. This behavior is in agreement with most other forms of atomization in that the droplet size decreases as the sole driving force for atomization increases. For this series of data, the sole driving force for atomization is the annular gas flow. The behaviors of the other two data series in Fig. 6 are different. For the two series reflecting needle gas flow rates of 144 and 338 ml/min, the decreases in SMD with annular gas flow rate are much smaller in magnitude. Neither series declines monotonically, and both exhibit inflection points.

These distinctions exceed the indicated error bars for the data. The different characteristics of the sprays produced by a single gas flow and those produced by two separate gas flows suggest that their atomization processes are different.

Similar trends are evident in Fig. 7. For the lowest annular gas flow rate (5003 ml/min), the SMD of the resulting spray decreases monotonically with increasing needle gas flow rate. Whereas no inflection points are evident for the lowest annular gas flow rate, they are apparent for the two higher annular gas flow rates. The decrease in SMD with increasing needle gas flow becomes less dramatic at higher annular gas flow rates. These characteristics support the observations from Fig. 6 that superposition of two driving forces modulates the atomization process. Figure 8 combines the data in Fig. 6 and Fig. 7, and incorporates additional data representing the lowest annular gas flow rates of this series of tests (0 and 2171 ml/min).

In the series having no annular gas flow (Fig. 8), the SMD values of the four lowest needle gas flow rates are nearly identical to each other and closely match the diameter of the fuel supply tube (OD = 3175 μm). The behavior of isopropyl alcohol as an injectant under these conditions is similar to that of water. In both cases, large droplets are discharged from a fluid meniscus at the exit of the fuel supply tube without undergoing further breakup at the needle tip (Fig. 2). Without the assistance of an annular gas flow, needle gas flow rates of up to 50 ml/min (41% of full scale) cannot break up the large droplets after they have separated from the meniscus. The three highest needle gas flow rates without annular gas flow (Fig. 8) succeed in breaking up the large droplets, producing sprays with SMDs less than the fuel supply tube diameter, which decrease with increasing needle gas flow. The second lowest annular gas flow rate (2171 ml/min) causes all needle gas flow rates to

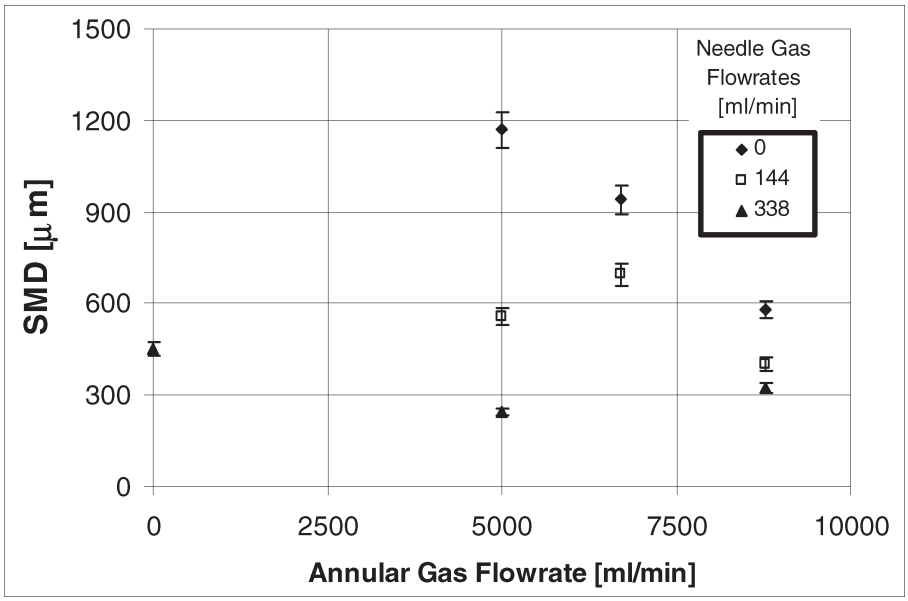

Fig. 6 Variation of Sauter mean diameter with annular gas flow rate for several different needle gas flow rates (isopropyl alcohol).

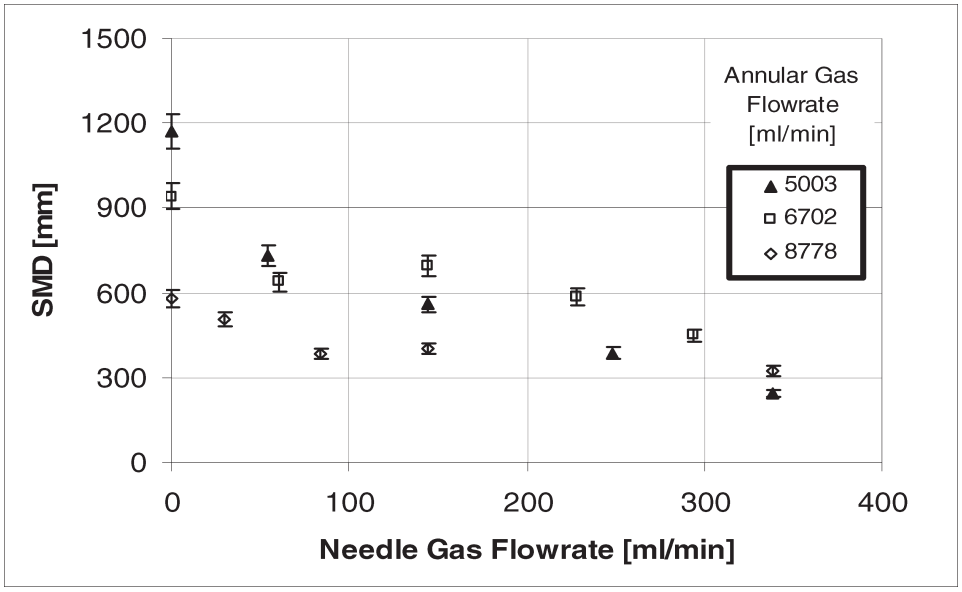

Fig. 7 Variation of Sauter mean diameter with needle gas flow rate for several different annular gas flow rates (isopropyl alcohol).

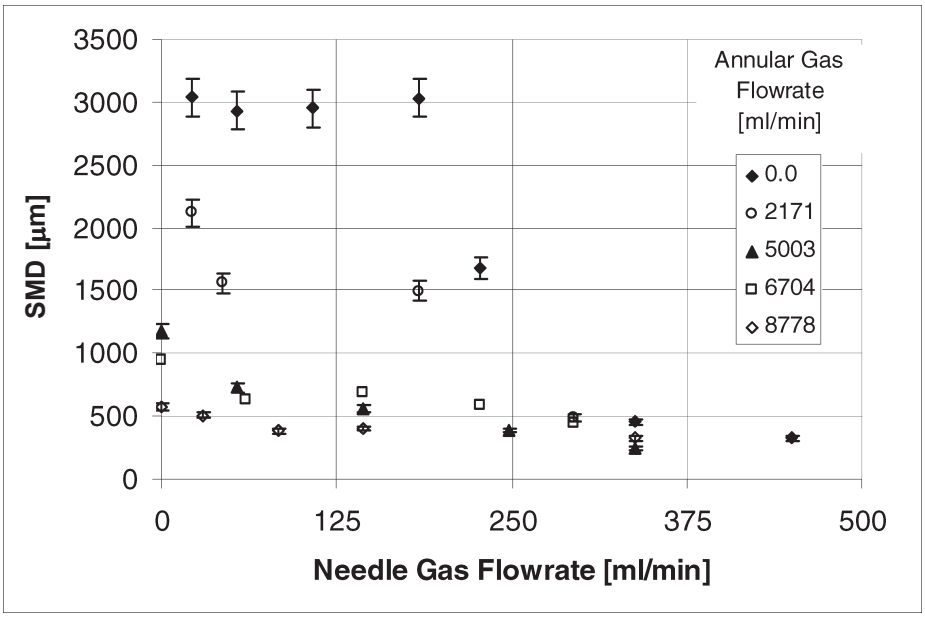

Fig. 8 Variation of Sauter mean diameter with needle and annular gas flow rates (isopropyl alcohol).

produce SMDs that are less than the diameter of the fuel supply tube. This markedly improved atomizer performance results from only a modest increase in annular gas flow (0 to 2171 ml/min, 17% of full scale), suggesting a change in the mode of atomization.

Spray Density Measurements

This study interrogates the spray with a 2-D planar light sheet. Quantifying spray density by measuring distances between droplets (linear, 2-D) naturally lends itself to this experimental method, just as diagnostics using probe volumes measure and report droplet number densities (volumetric, 3-D). The average distance between droplets varies inversely with spray density: as spray density increases, the spacing between droplets decreases. The *interdroplet spacing* represents the distance between two droplets i and j, and is symbolized here by L_{ij}. The interdroplet spacing between two droplets equals the distance between their centroids, less the sum of their radii (where radius is twice the feret diameter). The average value of L_{ij} between a droplet i and its P nearest neighboring droplets j within the spray is represented by $\bar{L}_{ij}(P)$. The average value of $\bar{L}_{ij}(P)$ over all droplets i in the spray equals the mean interdroplet spacing for the spray, $\bar{\bar{L}}_{ij}(P)$. This study primarily uses $\bar{\bar{L}}_{ij}(P)$ to characterize spray density. Mathematical definitions and brief descriptions of all spray density measures used in this study are presented in Table 2. A detailed discussion of the development of the L_{ij} -based spray density measures appears in the Appendix, including a demonstration of how average interdroplet spacing, as a spray density measure, compares to the more conventional droplet number density. This discussion includes a demonstration of how L_{ij}-based spray density measures compare to droplet number density in representing various droplet cluster configurations.

The interdroplet spacing data in Figs. 9–11 are normalized such that the resulting quantity $[\bar{\bar{L}}_{ij}(1)/\mathrm{SMD}]$ allows the comparison of spray density between sprays whose Sauter mean diameters differ. Note that interdroplet spacing $[\bar{\bar{L}}_{ij}(P)]$ is calculated with an index P equal to unity in Figs. 9–11, meaning that only the distances between each droplet and its nearest neighbor factor into the value of $\bar{\bar{L}}_{ij}(1)/\mathrm{SMD}$. The impact that larger values of P have on $\bar{\bar{L}}_{ij}(P)$ is discussed later in this section and in the Appendix. The data presented in normalized form in Figs. 9–11 are the same as those presented, unmodified, in Fig. 14 and Fig. 15 in the Appendix. The values of $\bar{\bar{L}}_{ij}(1)/\mathrm{SMD}$ in Fig. 9 vary more widely at the higher needle and annular gas flow rates than do the values of $\bar{\bar{L}}_{ij}(1)$ in Fig. 15 of the Appendix. Values of $\bar{\bar{L}}_{ij}(1)/\mathrm{SMD}$ in Fig. 9 vary by factors of 2 or more as annular and needle gas flow rates increase, clearly demonstrating variable control of normalized interdroplet spacing. Plotting the normalized value of the mean interdroplet spacing $[\bar{\bar{L}}_{ij}(1)/\mathrm{SMD}]$ versus the corresponding mean droplet size (SMD) for each data point produces a PFDAAA performance map, shown in Fig. 10. This performance map represents the operating range of the PFDAAA for the experimental conditions described. As the Mach numbers of the atomizing gas flows for these data are well below 0.01, higher atomizing gas supply pressures could increase the dynamic range of the PFDAAA considerably.

The following secondary analyses, conducted using a series of FORTRAN subroutines, evaluate alternative spray density measures or explore secondary effects. Earlier analyses used only the lower limiting value of $\bar{\bar{L}}_{ij}(P)$, namely, $\bar{\bar{L}}_{ij}(1)$. However, the behavior of $\bar{\bar{L}}_{ij}(P)$ for larger values of P is yet undefined. Two of the series in Fig. 11 address this

Table 2 Spray Density Parameters

Parameter	Mathematical definition[a–c]	Description
$\overline{L}_{ij}(N)$	$\overline{L}_{ij}(N)=\dfrac{\sum_j^N L_{ij}}{N}$	For a cluster of $N+1$ droplets, represents the average distance from a droplet i to every other droplet j in the image.
$\overline{\overline{L}}_{ij}(N)$	$\overline{\overline{L}}_{ij}(N)=\dfrac{\sum_i^{N+1}\left(\sum_j^N L_{ij}/N\right)}{N+1}$	For a cluster of $N+1$ droplets, represents the average over all $N+1$ droplets, of the average distance from each droplet i to every other droplet j in the image.
$\overline{\overline{L}}_{ij}(P)$	$\overline{\overline{L}}_{ij}(P)=\dfrac{\sum_i^{N+1}\left(\sum_j^P L_{ij}/P\right)}{N+1}$	For a cluster of $N+1$ droplets, represents the average over all $N+1$ droplets of the average distance from each droplet i to its P nearest neighboring droplets j.
$\overline{\overline{LM}}_{ij}(P)$	$\overline{\overline{LM}}_{ij}(P)=\dfrac{\sum_i^{N+1}\left\{\left[\sum_j^P L_{ij}(V_i)/V_j\right]/P\right\}}{N+1}$	A mass-weighted version of $\overline{\overline{L}}_{ij}(P)$. Distances from smaller droplets to larger droplets are reduced; distances from larger droplets to smaller droplets are increased.
$\overline{IFR}(P)$	For $L_{ij}/D_i < P$: $\overline{IFR}(P)=\dfrac{\sum_i^N\left(\sum_j V_j/V_i\right)}{N}$	Interacting fuel ratio (IFR): represents the total relative volume of liquid fuel suspended in droplets j within a nondime nsional radial distance R_{ij}/D_i of droplet i of volume V_i.

[a] L_{ij} represents the distance between the centroids of droplets i and j, less an amount equivalent to the sum of their radii. $L_{ij}(n)$ represents the distances to the n nearest droplets j to droplet i. For example, $L_{ij}(1)$ represents the distance from droplet i to its closest neighboring droplet j.

[b] V_i and V_j represent the fluid volumes of droplets i and j, respectively.

[c] D_i represents the diameter of droplet i.

deficiency, demonstrating the evolution of $\overline{\overline{L}}_{ij}(P)$ as P varies from unity to N for representative dense and a dilute spray conditions. The value of $\overline{\overline{L}}_{ij}(P)$ for the dense spray is consistently less than the value for dilute sprays over all values of P, indicating that the value of P does not influence the accurate representation of spray density.

Similar behavior is also evident for another spray density parameter, $\overline{\overline{LM}}_{ij}(P)$ (defined in Table 2), also plotted versus P in Fig. 11. The parameter $\overline{\overline{LM}}_{ij}(P)$ is a mass-weighted analog to $\overline{\overline{L}}_{ij}(P)$, and the motivation for its introduction stems from the following scaling arguments. Larger droplets induce larger thermal, species, and fluid dynamic wakes than smaller droplets in the medium that surrounds them. Consequently, a reasonable expectation is that the influence of larger droplets on nearby smaller droplets is greater than the influence of smaller droplets on nearby larger droplets. Introducing $\overline{\overline{LM}}_{ij}(P)$ provides

a spray density measure that can capture such secondary scaling effects that might arise in polydisperse droplet dispersions. Assuming the droplets have the same density, $\overline{\overline{LM}}_{ij}(P)$ accounts for the relative masses of the droplets by using the ratio of their volumes, V_i/V_j, as a weighting factor. The influence of this weighting factor is evident in Fig. 12, which shows how the ratio $LM_{ij}(P)/L_{ij}(P)$ varies with the ratio of droplet diameters, D_i/D_j, for a droplet pair. When measured from a smaller to a larger droplet ($D_i/D_j < 1$ in Fig. 12), the value of the mass-weighted interdroplet spacing [$LM_{ij}(P)$] is less than the unmodified interdroplet spacing [$\overline{\overline{L}}_{ij}(P)$]. From a larger droplet to a smaller droplet ($D_i/D_j > 1$ in Fig. 12), the value of the mass-weighted interdroplet spacing [$LM_{ij}(P)$] is greater than the unmodified interdroplet spacing [$L_{ij}(P)$]. For droplet pairs having identical diameters, the values of $LM_{ij}(P)$ and $L_{ij}(P)$ are equal. When plotted versus P in Fig. 11 for representative dense and dilute spray conditions, $\overline{\overline{LM}}_{ij}(P)$ consistently returns lower values for the denser spray condition and higher values for the more dilute spray condition. These results for $\overline{\overline{LM}}_{ij}(P)$ are consistent with those for $\overline{\overline{L}}_{ij}(P)$ over a large range of P, indicating that the dense and dilute sprays tested are distinct even when the effects of relative droplet size are considered.

The need to study interactions between vaporizing droplets [53–55] prompted the development of another spray density measure, the average interacting fuel ratio, $\overline{IFR}(P)$ (defined in Table 2). A locally dense dispersion of vaporizing droplets is likely to induce

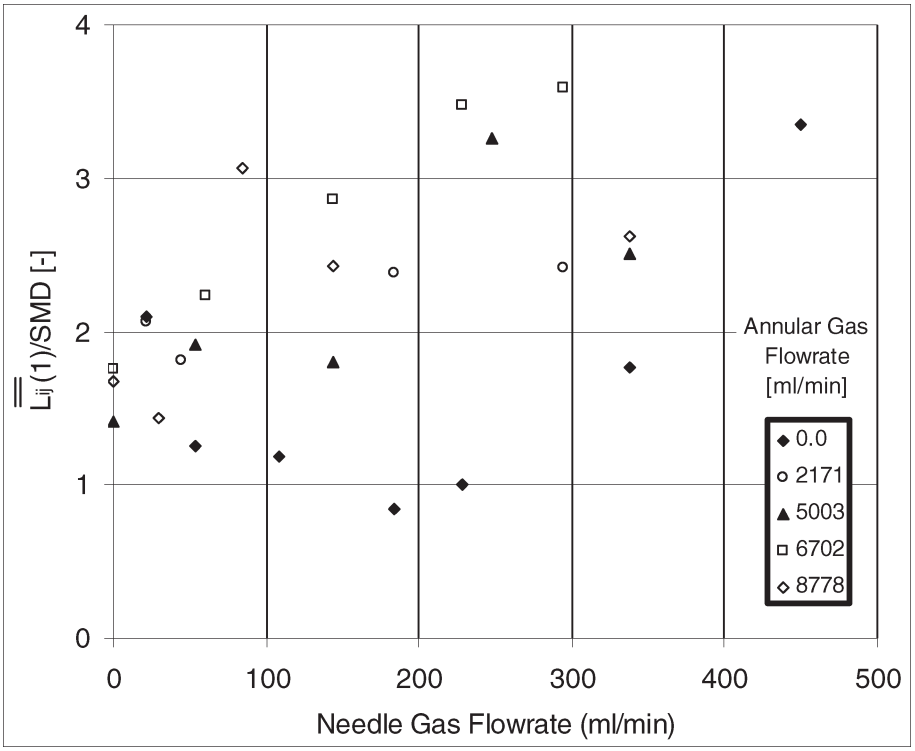

Fig. 9 Variation of normalized interdroplet spacing with needle and annular gas flow rates (isopropyl alcohol).

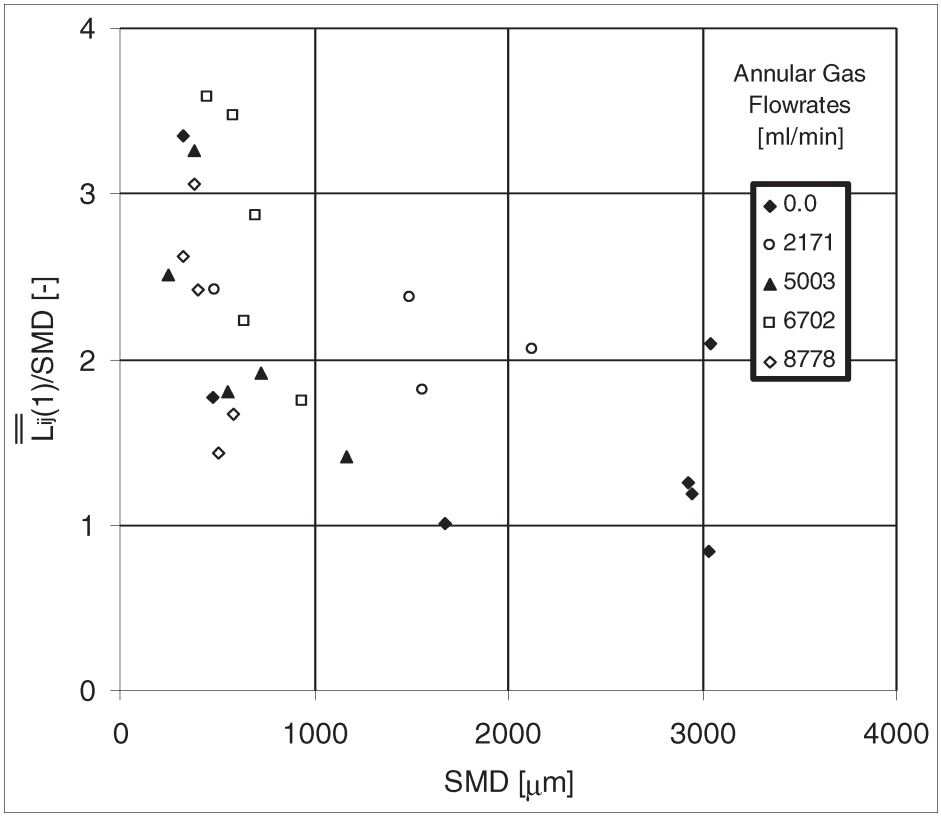

Fig. 10 Variation of normalized interdroplet spacing versus SMD (isopropyl alcohol).

locally lower temperatures and higher fuel vapor concentrations than a dilute dispersion. *IFR(P)* characterizes the potential for locally higher fuel vapor concentrations by calculating the total volume of liquid fuel within a specified radius of a vaporizing droplet *i*. *IFR(P)* is a ratio of two liquid volumes: the numerator is the volume of liquid collectively contained in all droplets *j* located within a sphere around droplet *i*; the denominator is the volume of droplet *i*. Unlike the interdroplet spacing parameters, for *IFR(P)* the index *P* controls the radius of the bounding sphere. For an arbitrary droplet *i* having diameter D_i, *IFR(P)* represents droplets within a bounding sphere of radius $r = P \cdot D_i$. $\overline{IFR}(P)$ is the average of *IFR(P)* over all droplets *i*. $\overline{IFR}(P)$ offers a redundant measure of spray density that is fundamentally different from the parameters that are derived from interdroplet distances. Values of $\overline{IFR}(P)$ for dense and dilute spray conditions (Fig. 11) indicate results that are consistent with other spray density measures over the entire range of *P*. Values of IFR are higher for dense spray conditions than for dilute spray conditions, reflecting the correct assertion that dense sprays contain a larger volume of liquid fuel within a given probe volume than dilute sprays.

All of these spray density measures—$\overline{\overline{L}}_{ij}(P)$, $\overline{\overline{LM}}_{ij}(P)$, and $\overline{IFR}(P)$—assume either quiescent conditions or negligible relative velocity (slip) between the gas and liquid phases.

For negligible slip, diffusion alone drives the omnidirectional propagation of temperature and concentration gradients around vaporizing droplets. Under these conditions, the likelihood of droplet interactions depends, to a first approximation, only on the radial separation distance between droplets. If negligible slip cannot be assumed, droplet interactions will no longer be omnidirectional, but will have a strong directional dependency that is aligned with the slip velocity vector. Under conditions of non-negligible slip, the omnidirectional spray density measures developed here would be inappropriate for characterizing the likelihood of droplet interactions.

Finally, Fig. 13 shows the variation of SMD versus the combined flow rate of the annular and needle gas flows at all tested operating points of the PFDAAA. The SMD for conventional air-blast atomizers varies continuously with the gas/liquid ratio (GLR), such as the results of Sakai et al. [58] that establish a relationship of the form SMD $\propto$ $(GLR)^{-0.75}$ using water as the injectant. That SMD for the PFDAAA varies discontinuously with the total flow rate of atomizing gas (proportional to GLR for the constant liquid flow rates maintained in this investigation) (Fig. 13) suggests the existence of multiple atomization modes. This behavior distinguishes PFDAAA operation from other air-blast or air-assist atomizers. The novelty of the PFDAAA design makes direct comparisons to other types of atomizers difficult. One atomizer that is reasonably similar is the prefilming air-blast atomizer of Rizkalla and Lefebvre [46]. The data in Fig. 13 compare measured PFDAAA performance (SMD) to predicted performance based on the correlation of Rizkalla and

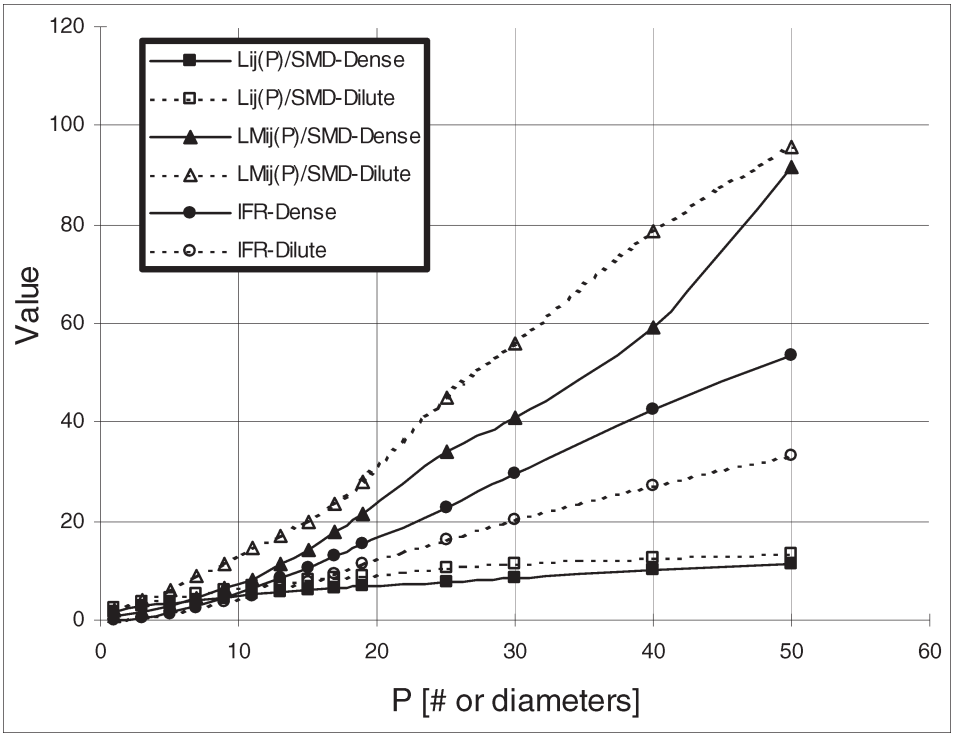

Fig. 11 Spray density measures L_{ij}, $\overline{\overline{LM}}_{ij}(P)$, and $\overline{IFR}(P)$ (isopropyl alcohol).

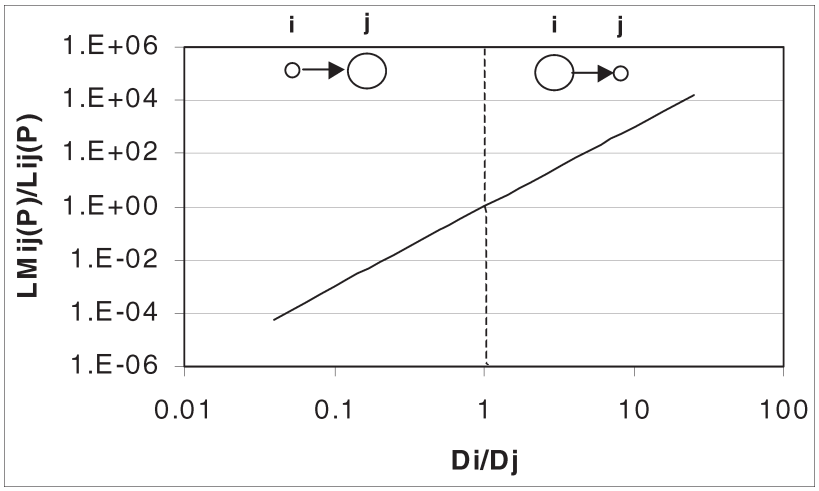

Fig. 12 Comparison of mass-weighted [$LM_{ij}(P)$] versus unweighted [$L_{ij}(P)$] interdroplet spacing measures, plotted versus droplet diameter ratio.

Lefebvre [46]. The correlation predicts lower values of SMD than were measured for the PFDAAA, and largely fails to capture the variation in SMD that occurs as the distribution of gas flowing through the PFDAAA changes. The differences, however, are not surprising, given the marked differences in the designs of the two atomizers (Fig. 13, right).

CONCLUSIONS

Independent control of mean droplet size and mean spray density for solid-cone liquid sprays is possible through a novel prefilming double-annular air-blast atomizer (PFDAAA) prototype. Two independently controlled gas streams induce separate but

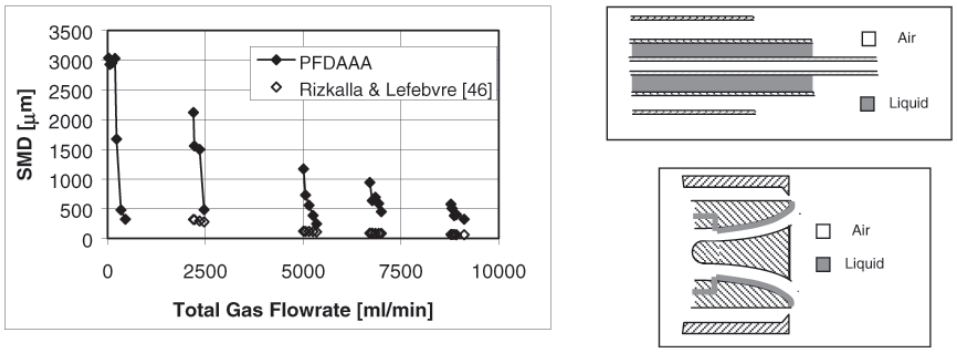

Fig. 13 Variation in SMD with total gas flow rate (left). Compares experimental data for PFDAAA (schematized, upper right) against correlation developed for the prefilming air-blast atomizer of Rizkalla and Lefebvre [46] (schematized, lower right).

complementary modes of atomization, as evidenced by the multiple curves relating mean droplet size and atomizing gas flow rate. Performance maps confirm the production of a range of spray densities for a single value of Sauter mean diameter. For the experimental conditions tested, values of SMD range from 250 to 3100 μm, and values of normalized interdroplet spacing range from 0.8 to 3.6 mean droplet diameters. In addition to controlling spray characteristics, the atomizer is designed to handle unpressurized injectants delivered at low fluid flow rates (1 ml/min or less). Higher atomizing gas pressures would likely reduce the SMD of the delivered spray and increase the dynamic range of operation. Parametrically variable sprays offer a new experimental approach to spray combustion research. Variable sprays provide the parametric control of single-droplet or droplet array studies, while maintaining the essential characteristics of practical sprays. When combined with laser-based spray diagnostics, changes in the internal physicochemical structure of a spray could be related to changes in bulk characteristics, thereby improving our understanding of internal spray processes.

REFERENCES

1. Lord Rayleigh, On the Instability of Jets, *Proc. Lond. Math. Soc.,* vol. 10, pp. 4–13, 1879.
2. G. I. Taylor, Generation of Ripples by Wind Blowing over a Viscous Fluid, in *The Scientific Papers of G. I. Taylor,* vol. III, pp. 244–254, 1940.**[[AU: PUBLISHER & PLACE OF PUBLICATION?]]**
3. G. I. Taylor, The Dynamics of Thin Sheets of Fluid III. Disintegration of Fluid Sheets, *Proc. R. Soc. Lond. A,* vol. 201, pp. 192–196, 1950.
4. N. Dombrowski and W. R. Johns, The Aerodynamic Instability and Disintegration of Viscous Liquid Sheets, *Chem. Eng. Sci.,* vol. 18, pp. 201–214, 1963.
5. C. J. Clark and N. Dombrowski, Aerodynamic Instability and Disintegration of Inviscid Liquid Sheet, *Proc. R. Soc. Lond. A,* vol. 392, pp. 467–478, 1972.
6. R. D. Reitz and F. V. Bracco, Mechanism of Atomization of a Liquid Jet, *Phys. Fluids,* vol. 25, p. 1730, 1982.
7. R. H. Rangel and W. A. Sirignano, Nonlinear Growth of Kelvin-Helmholtz Instability: Effect of Surface Tension and Density Ratio, *Phys. Fluids A,* vol. 31, pp. 1845–1855, 1988.
8. A. Mansour and N. Chigier, Disintegration of Liquid Sheets, *Phys. Fluids A,* vol. 2, pp. 706–718, 1990.
9. R. H. Rangel and W. A. Sirignano, The Linear and Nonlinear Shear Instability of a Fluid Sheet, *Phys. Fluids A,* vol. 3, pp. 2392–2400, 1991.
10. D. Sindayihebura and L. Bolle, Ultrasonic Atomization of Liquids: Stability Analysis of the Viscous Liquid Film Free Surface, *Atomization and Sprays,* vol. 8, pp. 217–233, 1998.
11. L.-P. Hsiang and G. M. Faeth, Near-Limit Drop Deformation and Secondary Breakup, *Int. J. Multiphase Flow,* vol. 13, pp. 741–757, 1987.
12. H. A. Stone, Dynamics of Drop Deformation and Breakup in Viscous Fluids, *Annu. Rev. Fluid Mech.,* vol. 26, pp. 65–102, 1994.
13. A. A. Shraiber, A. M. Podvysotsky, and V. V. Dubrovsky, Deformation and Breakup of Drops by Aerodynamic Forces, *Atomization and Sprays,* vol. 6, pp. 667–692, 1996.
14. J. Qian and C. K. Law, Regimes of Coalescence and Separation in Droplet Collision, *J. Fluid Mech.,* vol. 331, pp. 59–80, 1997.
15. M. Orme, Experiments on Droplet Collisions, Bounce, Coalescence, and Disruption, *Prog. Energy Combustion Sci.,* vol. 23, pp. 65–79, 1997.
16. Y. J. Jiang, A. Umemura, and C. K. Law, An Experimental Investigation on the Collision Behaviour of Hydrocarbon Droplets, *J. Fluid Mech.,* vol. 234, pp. 171–190, 1992.

17. G. A. E. Godsave, Studies of the Combustion of Drops in a Fuel Spray—The Burning of Single Drops of Fuel, *Proc. Combustion Inst.,* vol. 4, pp. 818–830, 1953.
18. D. B. Spalding, The Combustion of Liquid Fuels, *Proc. Combustion Inst.,* vol. 4, pp. 847–864, 1953.
19. G. Chen, S. K. Aggarwal, T. A. Jackson, and G. L. Switzer, Experimental Study of Pure and Multicomponent Fuel Droplet Evaporation in a Heated Air Flow, *Atomization and Sprays,* vol. 7, pp. 317–337, 1997.
20. I. Gokalp, C. Chauveau, H. Berrekam, and N. A. Ramos-Arroyo, Vaporization of Miscible Binary Fuel Droplets under Laminar and Turbulent Convective Conditions, *Atomization and Sprays,* vol. 4, pp. 661–676, 1994
21. J. S. Kim, A. Lee, and C. K. Law, On the Gasification of Droplets of Azeotropic Mixtures: Theory and Experiment, *Proc. Combustion Inst.,* vol. 23, pp. 1423–1429, 1990.
22. J. Y. Zhu and D. Dunn-Rankin, Temperature Characteristics of a Combusting Droplet Stream, *Proc. Combustion Inst.,* vol. 24, pp. 1473–1481, 1992.
23. N. Roth, A. Karl, K. Anders, and A. Frohn, Flame Propagation in Planar Droplet Arrays and Interaction Phenomena between Neighboring Droplet Streams, *Proc. Combustion Inst.,* vol. 26, pp. 1697–1703, 1996.
24. L. P. Gao, Y. D'Angelo, I. Silverman, A. Gomez, and M. D. Smooke, Quantitative Comparison of Detailed Numerical Computations and Experiments in Counterflow Spray Diffusion Flames, *Proc. Combustion Inst.,* vol. 26, pp. 1736–1746, 1996.
25. S. C. Li, P. A. Libby, and F. A. Williams, Experimental and Theoretical Studies of Counterflow Spray Diffusion Flames, *Proc. Combustion Inst.,* vol. 24, pp. 1503–1512, 1992.
26. T. Suzuki and H. H. Chiu, Multi-droplet Combustion of Liquid Propellants, *Proc. Ninth Int. Symp. Space Technology Science,* pp. 145–154, 1971.
27. H. H. Chiu and T. M. Liu, Group Combustion of Liquid Droplets, *Combustion Sci. Technol.,* vol. 17, pp. 127–142, 1977.
28. H. H. Chiu, H. Y. Kim, and E. J. Croke, Internal Group Combustion of Liquid Droplets, *Proc. Combustion Inst.,* vol. 19, pp. 971–980, 1982.
29. J. Xin and C. M. Megaridis, Modeling of Multiple Vaporizing Droplet Streams in Close Spacing Configurations, *Atomization and Sprays,* vol. 7, pp. 267–294, 1997.
30. H. H. Chiu and C. L. Lin, Anomolous Group Combustion of Premixed Clusters, *Proc. Combustion Inst.,* vol. 26, pp. 1653–1661, 1996.
31. J. Bellan and K. Harstad, Evaporation, Ignition and Combustion of Non-dilute Clusters of Drops, *Combustion and Flame,* vol. 79, pp. 272–286, 1990.
32. I. Silverman and W. A. Sirignano, Multi-droplet Interaction Effects in Dense Sprays, *Int. J. Multiphase Flow,* vol. 20, pp. 99–116, 1994.
33. H. A. Dwyer, H. Nirschl, P. Kerschl, and V. Denk, Heat, Mass, and Momentum Transfer about Arbitrary Groups of Particles., *Proc. Combustion Inst.,* vol. 25, pp. 389–395, 1994.
34. R. Borghi and S. Loison, Studies of Dense-Spray Combustion by Numerical Simulation with a Cellular Automaton, *Twenty-Fourth Symp. (Int.) on Combustion,* pp. 1541–1547, The Combustion Institute, Pittsburgh, PA, 1992.
35. J. Bellan and K. Harstad, Ignition of a Binary-fuel (Solvent-Solute) Cluster of Drops, *Combustion Sci. Technol.,* vol. 110–111, pp. 531–548, 1995.
36. J. Bellan, External Cluster Combustion of Binary-Fuel Drops, *Combustion Sci. Technol.,* vol. 120, pp. 213–236, 1996.
37. C. K. Law and H. K. Law, A d^2-Law for Multicomponent Droplet Vaporization and Combustion., *AIAA J.,* vol. 20, pp. 522–527, 1981.
38. C. M. Megaridis and W. A. Sirignano, Numerical Modeling of a Vaporizing Multicomponent Droplet, *Proc. Combustion Inst.,* vol. 23, pp. 1413–1421, 1990.
39. C. M. Megaridis and W. A. Sirignano, Multicomponent Droplet Vaporization in a Laminar Convective Environment, *Combustion Sci. Technol.,* vol. 87, pp. 27–44, 1992.

40. V. G. McDonnell, C. D. Cameron, and G. S. Samuelsen, Symmetry Assessment of an Air-Blast Atomizer Spray, *J. Propulsion,* vol. 6, pp. 375–381, 1990.
41. J.-J. Karl, D. Huilier, and H. Burnage, Mean Behavior of a Coaxial Air-Blast Atomized Spray in a Co-flowing Air Stream, *Atomization and Sprays,* vol. 6, pp. 409–433, 1996.
42. S. H. Song and S. Y. Lee, Study of Atomization Mechanism of Gas/Liquid Mixtures Flowing through Y-Jet Atomizers, *Atomizaation and Sprays,* vol. 6, pp. 193–209, 1996.
43. T. Sakai, D. Q. Zhao, M. Iijima, M. Saito, and M. Sato, Turbulence Characteristics of a Twin-Fluid Atomizer, *Atomization and Sprays,* vol. 6, pp. 577–600, 1996.
44. J. E. Beck, A. H. Lefebvre, and T. R. Koblish, Air-Blast Atomization at Conditions of Low Air Velocity, *J. Propulsion,* vol. 7, no. 2, pp. 207–212, 1991.
45. R. Aftel, A. K. Gupta, C. Cook, and C. Presser, Gas Property Effects on Droplet Atomization and Combustion in an Air-Assist Atomizer, *Proc. Combustion Inst.,* vol. 26, pp. 1645–1651, 1996.
46. A. A. Rizkalla and A. H. Lefebvre, Influence of Liquid Properties on Air-Blast Atomizer Spray Characteristics, *Trans. ASME, J. Eng. Power,* pp. 173–179, 1975.
47. S. K. Chen, A. H. Lefebvre, and J. Rollbuhler, Influence of Ambient Air Pressure on Effervescent Atomization, *J. Propulsion Power,* vol. 9, pp. 10–15, 1993.
48. J. S. Chin and A. H. Lefebvre, A Design Procedure for Effervescent Atomizers, *Trans. ASME,* vol. 117, pp. 266–271, 1995.
49. S. V. Sankar, D. M. Robart, and W. D. Bachalo, A Swirl Effervescent Atomizer for Spray Combustion, *Proc. ASME Heat Transfer Div.,* pp. 175–182, 1995.
50. F. Takahashi, W. J. Schmoll, and J. Dressler, Characteristics of a Velocity-Modulated Pressure-Swirl Atomizing Spray, *J. Propulsion Power,* vol. 11, pp. 955–963, 1995.
51. I. P. Chung, D. Dunn-Rankin, and A. Ganji, Characterization of a Spray from an Ultrasonically Modulated Nozzle, *Atomization and Sprays,* vol. 7, pp. 295–315, 1997.
52. J. S. Chin, N. K. Rizk, and M. K. Razdan, Effect of Inner and Outer Airflow Characteristics on High Liquid Pressure Prefilming Air-Blast Atomization, *J. Propulsion Power,* vol. 16, pp. 297–301, 2000.
53. H. L. Clack, C. P. Koshland, D. Lucas, and R. F. Sawyer, Observations of Spray Density Effects on Multicomponent Chlorinated Hydrocarbon Vaporization and Thermal Destruction, *Proc. Combustion Inst.,* vol. 27, pp. 1309–1316, 1998.
54. H. L. Clack, C. P. Koshland, D. Lucas, and R. F. Sawyer, Postflame By-product Formation from Size- and Density-Controlled 1,1,1-Trichloroethane Sprays, *Environ. Eng. Sci.,* vol. 16, pp. 177–185, 1999.
55. H. L. Clack, C. P. Koshland, D. Lucas, and R. F. Sawyer, On the Vaporization and Thermal Oxidation of Chlorinated Hydrocarbon/Alcohol Sprays, *Proc. Combustion Inst.,* vol. 28, in press.**[[AU: ADD YEAR & UPDATE IF POSSIBLE]]**
56. N. W. Sorbo, C. K. Law, D. P. Y. Chang, and R. R. Steeper, An Experimental Investigation of the Incineration and Incinerability of Chlorinated Alkane Droplets, *Proc. Combustion Inst.,* vol. 22, pp. 2019–2026, 1988.
57. N. W. Sorbo and D. P. Y. Chang, Observations of Chlorinated Hydrocarbon Droplet Gasification, *Combustion. Sci. Technol.,* vol. 85, pp. 419–435, 1992.
58. T. Sakai, M. Kito, M. Saito, and T. Kanbe, Characteristics of Internal Mixing Twin-Fluid Atomizer, *Proc. 1st Int. Conf. on Liquid Atomization Spray Systems (ICLASS),* pp. 235–241, 1978.

APPENDIX

This study uses the average distance between droplets, or *interdroplet spacing*, as an indicator of spray density. Interdroplet spacing, L_{ij}, is defined as the distance between the centroids of two droplets i and j, less the sum of their effective radii. The effective radius of a droplet is one-half of the effective diameter, or *feret diameter*. The feret diameter of an aspherical or irregularly shaped droplet equals the actual diameter of a spherical droplet having the same projected area. The image analysis algorithm automatically returns a null value for L_{ij} in the event that the calculated value is negative, as occasionally occurs for an irregularly shaped droplet pair in close proximity. Images containing only a single droplet require an alternative method of evaluating L_{ij}. We assume that a second droplet may exist just outside of the field of view. This hypothetical second droplet may fall anywhere along the image boundary, so we define L_{ij} for single droplets as the average distance from the droplet centroid to the image boundary. Defined in this way, the value of L_{ij} is constant (L_{ij} = 6375.6 μm) for a single droplet positioned anywhere within an image whose magnification and field of view are fixed. This value of L_{ij} is evident in Fig. 14, where the lowest annular and needle gas flow rates fail to atomize the injectant (see Fig. 8), resulting in images where only a single, large droplet is present. Although droplet deformation and coalescence are important aspects of sprays [14–16], the current study does not consider such phenomena.

In a dispersion consisting of $N + 1$ droplets, an arbitrary droplet i has N neighboring droplets and N values of L_{ij}. The variable $\bar{L}_{ij}(N)$ represents the average value of the interdroplet spacing between droplet i and each of its N neighbors The variable $\bar{\bar{L}}_{ij}(N)$ represents the average value of $\bar{L}_{ij}(N)$ for all N droplets. The data in Fig. 14 show that $\bar{\bar{L}}_{ij}(N)$ asymptotically approaches 3000 μm as needle gas flow rates increase. This asymp-

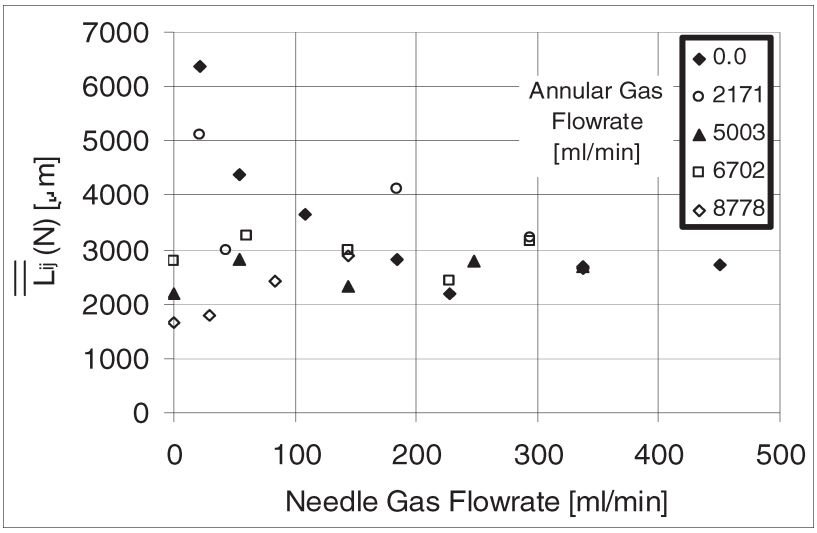

Fig. 14 Variation of $\bar{\bar{L}}_{ij}(N)$ with annular and needle gas flow rates (isopropyl alcohol).

totic behavior of $\bar{\bar{L}}_{ij}(N)$ at high needle gas flow rates is problematic. Figures 5–7 show that SMD decreases as needle and annular gas flow rates increase. The constant liquid injectant flow rate combined with the decreasing SMD translates into larger numbers of (smaller) droplets in each image as needle and annular gas flow rates increase. Increased numbers of droplets, contained within a fixed field of view, should result in the average distance between droplets decreasing as needle and annular gas flow rates increase. Thus, the asymptotic value approached by $\bar{\bar{L}}_{ij}(N)$ at higher needle gas flow rates in Fig. 14 suggests an overestimate of interdroplet spacing, and therefore an underrepresentation of spray density. One potential reason for this underrepresentation is that $\bar{L}_{ij}(N)$, used in calculating $\bar{\bar{L}}_{ij}(N)$, includes all possible droplet pairs. This implies, counterintuitively, that the nearest droplet j and the farthest droplet k exert equal influence on the physicochemical processes of arbitrary droplet i. To address this issue, we reduce the number of neighboring droplets j that are considered when calculating the average interdroplet spacing about an arbitrary droplet i. Instead of considering all N neighboring droplets j when calculating the average interdroplet spacing about arbitrary droplet i [$\bar{L}_{ij}(N)$], we choose to consider only P neighboring droplets j [$\bar{L}_{ij}(P)$], where P is any subset of N. Each droplet i in the dispersion has a unique value of $\bar{L}_{ij}(P)$ associated with the P nearest neighboring droplets, and the average value of $\bar{L}_{ij}(P)$ for all droplets in the dispersion is defined as $\bar{\bar{L}}_{ij}(P)$. When P takes on its minimum value ($P = 1$), the only interdroplet distance considered is that between an arbitrary droplet i and its single nearest neighboring droplet j. The different results obtained from using the maximum (N) and minimum (1) number of neighboring droplets when calculating interdroplet spacing are apparent in Fig. 14 $\bar{\bar{L}}_{ij}(N)$ and Fig. 15 [$\bar{\bar{L}}_{ij}(1)$].

The asymptotic value reached by all data as needle gas flow increases in Fig. 15 [$\bar{\bar{L}}_{ij}(1)$] is roughly one-third the corresponding value in Fig. 14 [$\bar{\bar{L}}_{ij}(N)$]. This difference clearly shows how consideration of all possible droplet pairs in a dispersion inflates the value of average interdroplet spacing, particularly as finer atomization occurs and SMD decreases. The overall trend of the data in Fig. 15 is decreasing average interdroplet spacing as needle gas flow rate increases, which is intuitively consistent with increasingly fine atomization at a constant injectant flow rate.

Droplet number density is the more conventional method of measuring spray density. The schematic diagrams in Fig. 16 allow direct comparison of the manner in which $\bar{\bar{L}}_{ij}(1)$, $\bar{\bar{L}}_{ij}(N)$, and droplet number density (DND) represent changes in spray density for six different droplet configurations. The baseline configuration in Fig. 16 is eight droplets located at the corners of a cube measuring 1 cm on a side. Figures 16a–16c examine how $\bar{\bar{L}}_{ij}(N)$, $\bar{\bar{L}}_{ij}(1)$, and DND vary as a single droplet is added to the cube volume in three different locations: at the center of the cube (Fig. 16a), at the center of a face (Fig. 16b), and at the middle of an edge (Fig. 16c). Figures 16d–16f examine a similar scenario with three droplets added in the same locations: along a cube diagonal (Fig. 16d), along a face diagonal (Fig. 16e), and along an edge (Fig. 16f). The results show that the location of the added droplet(s) does not change the droplet number density: the DND for Figs. 16a–16c is 9 cm^{-3} and is 11 cm^{-3} for Figs. 16d–16f. The variations of $\bar{\bar{L}}_{ij}(N)$ and $\bar{\bar{L}}_{ij}(1)$ make it clear that average interdroplet spacing is a more sensitive measure of spray density. The value of $\bar{\bar{L}}_{ij}(N)$ increases as the ninth droplet moves from the cube center successively to a cube face and to a cube edge (Figs. 16a–16c). In contrast, the value of $\bar{\bar{L}}_{ij}(1)$ decreases in Figs. 16a–

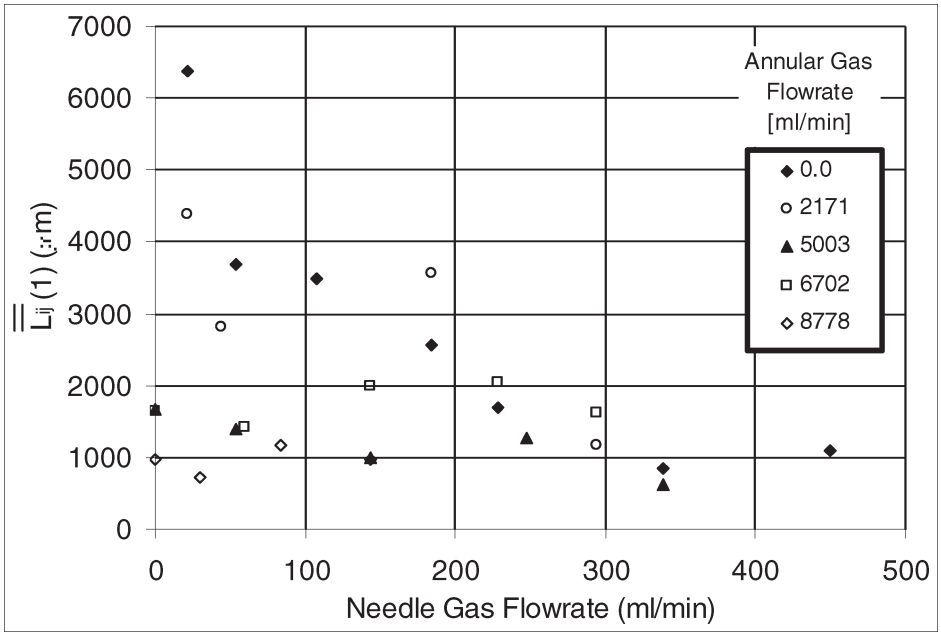

Fig. 15 Variation of $\bar{\bar{L}}_{ij}(1)$ with annular and needle gas flow rates (isopropyl alcohol).

16c. The different trends highlight the differences between $\bar{\bar{L}}_{ij}(N)$ and $\bar{\bar{L}}_{ij}(1)$. The inclusion of all possible droplet pairs in calculating the average interdroplet spacing contributes to the increase in $\bar{\bar{L}}_{ij}(N)$. The changing position of the ninth droplet changes the interdroplet spacing for eight of the 72 possible droplet pairs, producing a change in $\bar{\bar{L}}_{ij}(N)$. On the other hand, $\bar{\bar{L}}_{ij}(1)$ incorporates only the interdroplet spacing between a droplet and its closest neighbor. The eight droplets of the baseline configuration each are 1 cm distant from their closest neighbor; thus, the ninth droplet primarily influences $\bar{\bar{L}}_{ij}(1)$ only when its position is less than 1 cm from one of its neighbors. Successively fewer droplets in the baseline configuration meet this criterion in the sequence of configurations shown in Figs. 16a–16c, however, those that do comprise droplet pairs whose interdroplet distances are shrinking. The net result is that as the ninth droplet moves through the sequence of configurations shown in Figs. 16a–16c, $\bar{\bar{L}}_{ij}(1)$ decreases. A similar analysis for Figs. 16d–16f reveals largely similar trends. The addition of three droplets yields a constant value of droplet number density regardless of their orientation within the baseline configuration. As the orientation of the three additional droplets changes successively from the cube body diagonal, to a face diagonal, and finally to an edge, the value of $\bar{\bar{L}}_{ij}(N)$ increases in a manner similar to that found in Figs. 16a–16c. The value of $\bar{\bar{L}}_{ij}(1)$, however, also increases over this same sequence, a contradictory trend to that shown in Figs. 16a–16c. However, because this increase is an order of magnitude smaller than that observed Figs. 16a–16c, a reasonable characterization would be that $\bar{\bar{L}}_{ij}(1)$ is constant for the sequence shown in Figs. 16d–16f. The essential difference in the behavior of $\bar{\bar{L}}_{ij}(1)$ for a single added droplet as compared to three added droplets is the initial value of $\bar{\bar{L}}_{ij}(1)$ in each case. For a single

added droplet at the cube center (Fig. 16a), the value of $\bar{\bar{L}}_{ij}(1)$ is relatively large, allowing for significant reduction as the ninth droplet moves to the face or edge of the cube. For three droplets added along a cube diagonal (Fig. 16d), the value of $\bar{\bar{L}}_{ij}(1)$ is smaller, owing to the proximity of the first and last droplets on the diagonal to the corners of the cube. Because $\bar{\bar{L}}_{ij}(1)$ is initially small, there is less potential for further reduction and consequently $\bar{\bar{L}}_{ij}(1)$ appears largely insensitive to changes in the locations of the three added droplets. From these comparisons, we conclude that average interdroplet spacing captures differences in droplet cluster configurations that the more conventional measure of droplet number density cannot. Thus, interdroplet spacing is well suited to serve as a measure of spray density and as a gauge of droplet interactions within sprays.

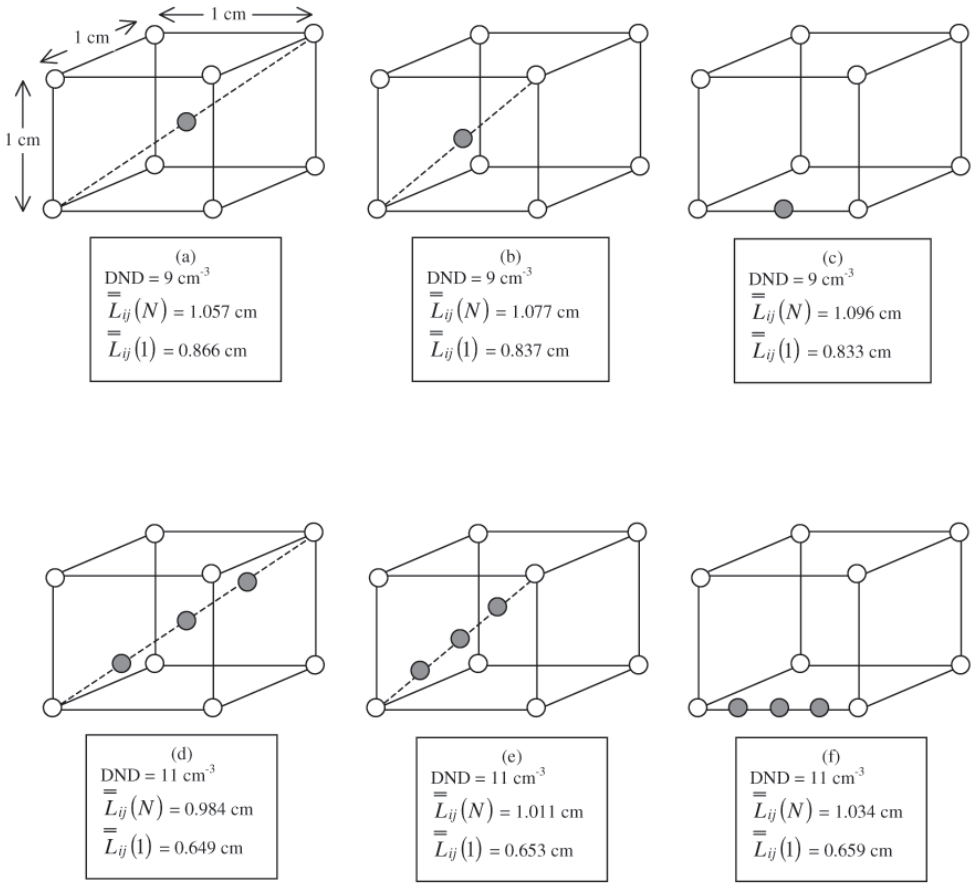

Fig. 16 Comparison of $\bar{\bar{L}}_{ij}(N)$ and $\bar{\bar{L}}_{ij}(1)$ values to droplet number density for six different droplet configurations.